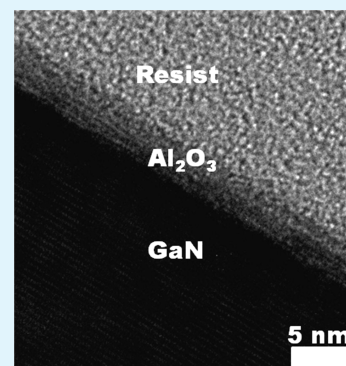


# Surface Passivation of Gallium Nitride by Ultrathin RF-Magnetron Sputtered Al<sub>2</sub>O<sub>3</sub> Gate

Hock Jin Quah and Kuan Yew Cheong\*

Electronic Materials Research Group, School of Materials & Mineral Resources Engineering, Engineering Campus, Universiti Sains Malaysia, 14300 Nibong Tebal, Seberang Perai Selatan, Penang, Malaysia

**ABSTRACT:** An ultrathin RF-magnetron sputtered Al<sub>2</sub>O<sub>3</sub> gate on GaN subjected to postdeposition annealing at 800 °C in O<sub>2</sub> ambient was systematically investigated. A cross-sectional energy-filtered transmission electron microscopy revealed formation of crystalline Al<sub>2</sub>O<sub>3</sub> gate, which was supported by X-ray diffraction analysis. Various current conduction mechanisms contributing to leakage current of the investigated sample were discussed and correlated with metal-oxide-semiconductor characteristics of this sample.



**KEYWORDS:** gallium nitride, aluminum oxide, conduction mechanisms, passivation, oxygen

## INTRODUCTION

A dramatic upsurge in demand of energy consumption throughout the world has hastened the momentum in developing next-generation metal-oxide-semiconductor (MOS) devices for high-power and high-temperature applications using gallium nitride (GaN) as the semiconductor substrate. GaN is ideally suited for these applications because of its wide bandgap (3.4 eV), large critical electric field (3 MV/cm), high electron mobility, as well as good thermal conductivity and stability.<sup>1,2</sup> To produce an energy-efficient GaN-based MOS device, a high-quality gate oxide is of prior concern to achieve low leakage current and high transverse electric field of the devices.<sup>2</sup> Relatively low dielectric constant ( $k$ ) and high- $k$  gate oxides have been extensively investigated on the GaN.<sup>1,2</sup> The relatively low- $k$  gate oxides, such as SiN<sub>x</sub>O<sub>y</sub> ( $k = 5.0$ – $7.5$ ) or SiO<sub>2</sub> ( $k = 3.9$ )<sup>2</sup> with low dielectric breakdown field ( $E$ ) may not assist in fabricating energy efficient GaN-based MOS devices. Breakdown of the devices is constrained by shortcomings of SiN<sub>x</sub>O<sub>y</sub> or SiO<sub>2</sub> gate rather than exploiting high  $E$  possessed by the GaN substrate. This inadequacy can be prevailed using high- $k$  gate oxides in the GaN-based MOS devices.

Particular interest has developed toward utilizing aluminum oxide (Al<sub>2</sub>O<sub>3</sub>;  $k = 8$ – $10$ ) as a high- $k$  gate in the GaN-based MOS devices in recent times.<sup>3,4</sup> This is owing to the presence of the Al<sub>2</sub>O<sub>3</sub> gate in amorphous phase regardless of deposition techniques and ambient.<sup>3–6</sup> The amorphous phase was preserved after postdeposition annealing (PDA) at 800 °C.<sup>4,5</sup> The lowest interface trap density, the smallest hysteresis, and the lowest leakage current density ( $J$ ) were attained by the amorphous Al<sub>2</sub>O<sub>3</sub> formed at 800 °C.<sup>4,5</sup> However, Toyoda et al. reported transformation of the amorphous phase to crystalline

phase at this temperature (800 °C).<sup>6</sup> The crystalline Al<sub>2</sub>O<sub>3</sub> formed at 800 °C has demonstrated larger band gap ( $E_g = 8.3$  eV) and conduction band offset with respect to GaN ( $\Delta E_c = 3.5$  eV) when compared with the amorphous Al<sub>2</sub>O<sub>3</sub> ( $E_g = 7.6$  eV and  $\Delta E_c = 2.7$  eV).<sup>6</sup> Acquisition of larger  $E_g$  and  $\Delta E_c$  for the crystalline Al<sub>2</sub>O<sub>3</sub> is anticipated to provide better electrical performance since conduction of charges through the conduction band of the oxide would be impeded though literatures<sup>4,5</sup> reported that the  $J$  was deteriorated at PDA beyond 800 °C due to presence of the crystalline Al<sub>2</sub>O<sub>3</sub>. In this work, crystalline Al<sub>2</sub>O<sub>3</sub> was formed on GaN substrate during PDA at 800 °C in oxygen (O<sub>2</sub>) ambient. A better  $J$ – $E$  characteristic of the crystalline Al<sub>2</sub>O<sub>3</sub> is shown in Figure 1 in comparison with replotted  $J$ – $E$  characteristics of formerly reported Al<sub>2</sub>O<sub>3</sub>/GaN<sup>3,7–12</sup> structure using linear approximation method. Besides, the obtained  $J$ – $E$  characteristic in this work has surpassed the  $J$ – $E$  characteristics demonstrated by majority reported gate oxide materials.<sup>2</sup> A detailed analysis on the structural and electrical performance of Al<sub>2</sub>O<sub>3</sub>/GaN structure that contributed to this observation has been provided in this letter.

## EXPERIMENTAL SECTION

Commercially purchased Si-doped (n-type) GaN epitaxial layer [7 μm thick and doping concentration of  $(1$ – $9) \times 10^{18}$  cm<sup>-3</sup>] grown on sapphire substrate was RCA cleaned prior to deposition of Al<sub>2</sub>O<sub>3</sub> film (~ 6 nm) using RF-magnetron sputtering system (HHV Auto500). Deposition parameters reported in previous work<sup>2</sup> at a power of 160

Received: June 16, 2013

Accepted: July 22, 2013

Published: July 22, 2013

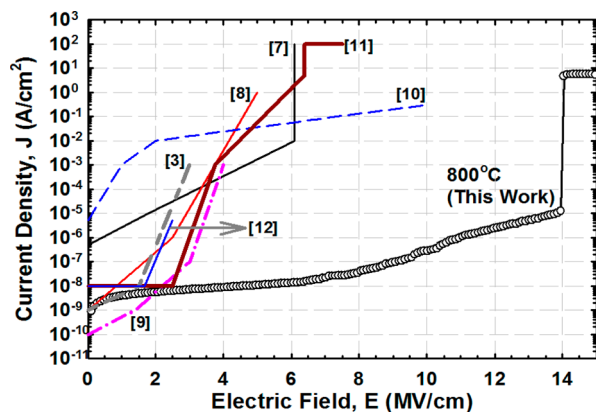


**Figure 1.** Comparison of  $J$ - $E$  characteristics of reported  $\text{Al}_2\text{O}_3/\text{GaN}$  system.

We were used during deposition of the  $\text{Al}_2\text{O}_3$  film. PDA at  $800^\circ\text{C}$  (heating and cooling rate =  $10^\circ\text{C}/\text{min}$ ) in  $\text{O}_2$  ambient for 30 min was performed in horizontal tube furnace. The  $\text{Al}_2\text{O}_3$  layer was selectively etched by  $\text{HF}:\text{H}_2\text{O}$  solution and Al was evaporated on top of the oxide using thermal evaporator (AUTO 306). Subsequently, an array of  $2.5 \times 10^{-3} \text{ cm}^2$  Al gate electrode was defined using photolithography process. Figure 2 shows a schematic illustration of the fabricated Al/

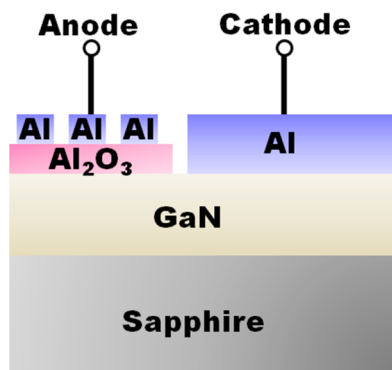


**Figure 2.** Schematic illustration of Al/ $\text{Al}_2\text{O}_3/\text{GaN}$ -based MOS structure.

$\text{Al}_2\text{O}_3/\text{GaN}$ -based MOS structure. Physical characteristics of the oxide were analyzed using energy-filtered transmission electron microscopy (EFTEM; Zeiss LIBRA 200) and X-ray diffraction (XRD; P8 Advan-Bruker). Gate thickness and refractive index were estimated at 5 different locations using MProbe thin film measurement system (Semiconsoft UVVisSR) at a wavelength of 632.8 nm. High frequency (HF; 100 kHz) capacitance-voltage ( $C$ - $V$ ) and current-voltage ( $I$ - $V$ ) characteristics of the MOS test structures were measured by Keithley 4200-SCS and Agilent 4156C, respectively.

## RESULTS AND DISCUSSION

EFTEM image of RF-magnetron sputtered  $\text{Al}_2\text{O}_3$  gate on GaN, which has been subjected to PDA at  $800^\circ\text{C}$  is shown in inset of Figure 3. Detection of fringes in region of  $\text{Al}_2\text{O}_3$  gate revealed the formation of crystalline structure, which was supported from XRD with the detection of  $\text{Al}_2\text{O}_3$  phase (ICDD file no. 01-074-0323) oriented in (110) and (024) planes (not shown). Besides, EFTEM also disclosed the absence of interfacial layer (IL) in the  $\text{Al}_2\text{O}_3/\text{GaN}$  system. XRD supported this claim since no  $\beta\text{-Ga}_2\text{O}_3$  phase was detected, wherein crystalline  $\beta\text{-Ga}_2\text{O}_3$  phase is formed at  $800^\circ\text{C}$ .<sup>2</sup> The absence of IL in this work is in agreement with the reported atomic-layer-deposited (ALD)  $\text{Al}_2\text{O}_3$  on GaN PDA at  $800^\circ\text{C}$ .<sup>3</sup> Average

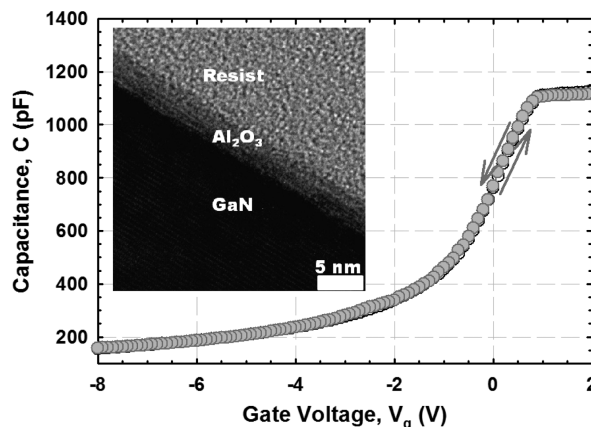


**Figure 3.**  $C$ - $V$  curve of Al/ $\text{Al}_2\text{O}_3/\text{GaN}$ -based MOS structure. Inset shows cross-sectional EFTEM image of  $\text{Al}_2\text{O}_3/\text{GaN}$  system.

measured thickness of the  $\text{Al}_2\text{O}_3$  gate at 20 different locations from the EFTEM (3.6 nm) is comparable with that acquired from MProbe ( $\sim 4.4$  nm).

Figure 3 presents the HF  $C$ - $V$  measurement of this sample, which is swept bidirectionally from  $-8$  to  $+2$  V. Deep depletion is observed in negative bias because of the slow generation rate of minority carriers at room temperature by the GaN. A negative flatband voltage shift ( $\Delta V_{\text{FB}}$ ) is perceived, indicating existence of positively charged traps in the oxide. This is shown via acquisition of a positive effective oxide charge,  $Q_{\text{eff}}$  of  $2.1 \times 10^{12} \text{ cm}^{-2}$  in the oxide, which is comparable with reported values of ALD  $\text{Al}_2\text{O}_3$  ( $1.2$ - $1.3 \times 10^{12} \text{ cm}^{-2}$ ) on GaN.<sup>4,13</sup> A minute hysteresis in the  $C$ - $V$  curves (Figure 3) indicates existence of slow trap with density of  $1.1 \times 10^{11} \text{ cm}^{-2}$  in this oxide. Presence of donor traps in the oxide may contribute to this, whereby tendency to capture and release injected electrons from the traps in the oxide is low. Terman's method<sup>14</sup> was used to extract interface trap density ( $D_{\text{it}} = 1.1 \times 10^{13} \text{ cm}^{-2} \text{ eV}^{-1}$  at  $E_c - E_t = 0.50 \text{ eV}$ ), which is comparable with density reported by ALD  $\text{Al}_2\text{O}_3$  ( $\sim 1.0 \times 10^{13} \text{ cm}^{-2} \text{ eV}^{-1}$ )<sup>3</sup> at similar  $E_c - E_t$ .

Figure 4 shows  $J$ - $E$  characteristics of this sample measured at  $25$ - $175^\circ\text{C}$ . Current conduction behavior for this sample adheres to Lampert's theory of space-charge-limited conduction (SCLC) at low  $V_g$ , which is bounded by 3 regions known as Ohm's law ( $J_{\text{ohm}} = qn_0\mu(V_g/d)$ ), SCLC that follows Mott-Gurney law ( $J_{\text{Mott-Gurney}} = 9\epsilon_r\epsilon_0\mu V_g^2/8d^3$ ), and trap-filled-limit

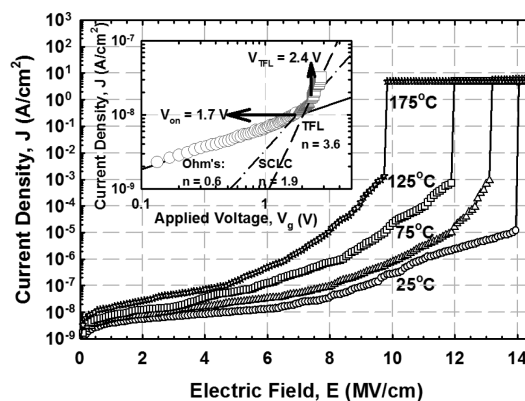


**Figure 4.**  $J$ - $E$  characteristic of  $\text{Al}_2\text{O}_3/\text{GaN}$  MOS capacitor measured from  $25$  to  $175^\circ\text{C}$ . Inset shows a typical space-charge-limited conduction plot of this sample measured at  $25^\circ\text{C}$ .

conduction (TFL;  $J_{\text{TFL}} = B(V_g^n/d^{2l+1})$ ); where  $q$ ,  $n_o$ ,  $\mu$ ,  $V_g$ ,  $d$ ,  $\epsilon_p$ ,  $\epsilon_o$ ,  $B$  and  $l$  are electronic charge, free charge carriers concentration in thermal equilibrium, charge carrier mobility in  $\text{Al}_2\text{O}_3$ , gate voltage,  $\text{Al}_2\text{O}_3$  gate thickness, dynamic dielectric constant, permittivity of free space, a constant, and a constant related to trap distribution and temperature, respectively.<sup>15</sup> Acquisition of a gradient (0.6–0.7) extracted from the  $\log(J) - \log(V_g)$  (inset of Figure 4) at low  $V_g$  indicates occurrence of Ohmic conduction, which is comparable to 1. When the  $V_g$  approaches  $V_{\text{on}}$ , carrier transit time ( $\tau_c = d^2/\mu V_{\text{on}}$ ) is equal to dielectric relaxation time ( $\tau_d = \epsilon_r \epsilon_o / qn\mu$ ).<sup>15</sup> At  $V_g \geq V_{\text{on}}$ , SCLC is dominating the current conduction as the extracted gradient (1.8–2.4) is close to 2. Because  $V_{\text{on}}$  (0.8–1.7 V) and  $\tau_c$  [(1.2–1.3)  $\times 10^{-2}$  s] are identified,  $\mu$  [(0.6–1.4)  $\times 10^{-11}$   $\text{cm}^2 \text{V}^{-1} \text{s}^{-1}$ ] in  $\text{Al}_2\text{O}_3$  gate is determined. Further increase in the  $V_g$  to TFL voltage ( $V_{\text{TFL}} = qN_t d^2 / 2\epsilon_r \epsilon_o$ ) leads to a shift from SCLC to TFL conduction and the extracted gradient from TFL region is 3.5–6.2. A reduction in  $V_{\text{TFL}}$  from 2.4 to 1.7 V with respect to measurement temperature suggests that higher temperature has triggered thermally generated carriers to occupy the available traps in the oxide. Density of traps ( $N_t$ ) present in the oxide is (4.5–6.5)  $\times 10^{19} \text{ cm}^{-3}$ . A reduction in the  $N_t$  with the increase in measurement temperature has enhanced number of free moving carriers in the oxide, which is related to the increment in  $\mu$ . The attainment of a higher  $\mu$  and  $N_t$  have resulted in an increase in  $J$  at higher measurement temperature.

Beyond TFL region, Schottky Emission (SE), Poole–Frenkel (PF) emission, and Fowler–Nordheim (FN) tunneling could be the governing conduction mechanisms. Datafit version 9.0.59 was used to perform a nonlinear curve fitting on the acquired  $J$ – $E$  results with these conduction mechanisms. SE is termed as thermionic emission of electrons over the oxide–GaN surface barrier.<sup>16</sup> Obtained experimental  $J$ – $E$  results that are fitted well with SE are shown in Figure 5. SE is deemed to be the dominating

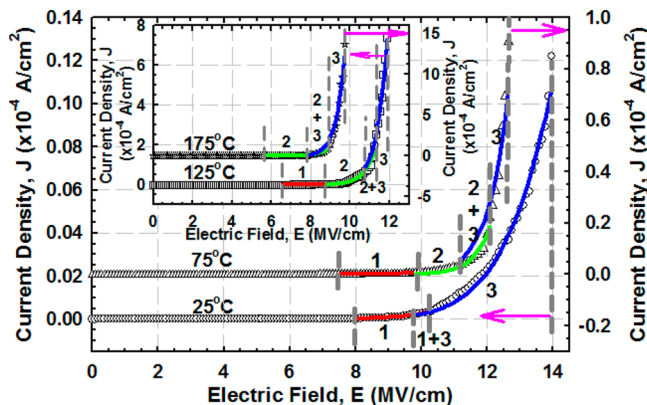


**Figure 5.** Experimental data (symbol) for sample measured at 25–75 °C and 125–175 °C (inset) fitted well with SE (red line), PF emission (green line), and FN tunneling (blue line) models. The numbering 1–3 represents dominance of SE, PF emission, and FN tunneling, respectively.

conduction when the extracted  $\epsilon_r$  value is comparable with optical dielectric constant ( $\epsilon_{\text{opt}}$ ) of the film, [ $\epsilon_r^{1/2} = \epsilon_{\text{opt}}^{1/2} = n$ , where  $n$  is the refractive index of the film ( $n = 1.69$ – $1.78$ )] and the nonlinear curve fitting yields a coefficient of determination,  $r^2$  of higher than 0.75. The  $J$  of this sample is governed by SE at measurement temperature from 25 to 125 °C (Figure 5) and the extracted  $\epsilon_r^{1/2}$  is 1.92–2.22. An increment in barrier height ( $\Phi_B = 1.052$ – $1.224$  eV) as a function of measurement

temperature denotes triggering of electron emission to overcome a higher surface barrier with the enhancement of measurement temperature, which leads to stimulation of  $J$ .

When  $E$  is further enhanced, PF emission is governing the  $J$  and region fitted well with PF emission model is shown in Figure 5. Trap energy level ( $\Phi_t = 1.506$ – $1.584$  eV) is obtained for sample measured from 75 to 175 °C as the attained  $\epsilon_r^{1/2}$  (1.63–1.90) value is comparable with  $n$ . An increment in the measurement temperature has contributed to a rise in the  $\Phi_t$ , whereby the carriers trapped by the traps that are located deeper in the oxide is released. The positive  $Q_{\text{eff}}$  present in the oxide is postulated to cause PF emission to occur. Initially, the positive  $Q_{\text{eff}}$  will capture the injected electrons to form neutral traps. Tendency of detrapping the charges from the positive  $Q_{\text{eff}}$  through PF emission is low. Hence, a higher  $E$  and measurement temperature is required for this process to happen than SE.

FN tunneling, which is a tunneling process that allows injected charged carriers to pass through triangular energy barrier into conduction band of the  $\text{Al}_2\text{O}_3$  gate<sup>16</sup> has been used to determine  $\Phi_B$  between the  $\text{Al}_2\text{O}_3$  gate and GaN, in which the  $\Phi_B$  is referred to as the conduction band offset ( $\Delta E_c$ ) between the  $\text{Al}_2\text{O}_3$  gate and GaN. Figure 5 shows regions fitted well with the model. The  $\Phi_B$  value estimated from FN tunneling is 2.97–4.81 eV at 25–175 °C, which is higher than that obtained from SE. The attainment of a higher  $\Phi_B$  from FN tunneling is due to the occurrence of this mechanism at a higher  $E$ , wherein the slope of energy band in the  $\text{Al}_2\text{O}_3$  gate and GaN becomes steeper. The obtained  $\Phi_B$  (2.97 eV) at 25 °C in this work is larger than the reported  $\Phi_B$  for ALD  $\text{Al}_2\text{O}_3$  (2.20 eV)<sup>3</sup> and metal–organic decomposed  $\text{CeO}_2$  (1.13 eV) spin-coated<sup>17</sup> on GaN. Unfortunately, the obtained  $\Phi_B$  (2.97 eV) from FN tunneling model in this work is lower than the computed  $\Delta E_c$  of chemical vapor deposited  $\text{Al}_2\text{O}_3$  on GaN (3.50 eV)<sup>6</sup> subjected to similar PDA temperature using X-ray absorption spectroscopy (XAS). A discrepancy of 0.53 eV between the acquired  $\Delta E_c$  may be related to the usage of extraction methods. This could be supported based on previous investigations, wherein a difference of 0.50 eV has been determined between the  $\Delta E_c$  attained using FN tunneling model for the as-deposited  $\text{Al}_2\text{O}_3$  gate using ALD on GaN (2.20 eV)<sup>3</sup> and the  $\Delta E_c$  acquired using XAS for the as-deposited  $\text{Al}_2\text{O}_3$  gate using CVD on GaN (2.70 eV).<sup>6</sup> When XAS and ultraviolet photoelectron spectroscopy (UPS) characterizations are utilized to compute the  $\Delta E_c$  for CVD (2.80 eV)<sup>6</sup> and ALD (3.00 eV)<sup>18</sup>  $\text{Al}_2\text{O}_3$  gate on GaN substrate, respectively, subjected to postdeposition annealing (PDA) at 700 °C, the acquired  $\Delta E_c$  values did not differ appreciably. This indicates that extraction of  $\Delta E_c$  value using FN tunneling model may differ considerably with a limit of approximately 0.5 eV from XAS/UPS characterization. Thus, it is believed that the quality of RF-magnetron sputtered  $\text{Al}_2\text{O}_3$  gate on GaN substrate in this work is comparable with CVD  $\text{Al}_2\text{O}_3$  gate on GaN substrate<sup>6</sup> yet better than ALD  $\text{Al}_2\text{O}_3$  gate on GaN.<sup>3</sup> A combination of SE and FN tunneling as well as PF emission and FN tunneling mechanisms governing the  $J$  of investigated sample at 25 °C and 75–175 °C, respectively, has been also shown in Figure 5.

Based on the aforementioned discussion, the  $\text{Al}_2\text{O}_3$  gate, which has been RF-magnetron sputtered on GaN substrate could serve as a good passivation layer. This is supported through the acquisition of a higher  $\Phi_B$  using FN tunneling model for the RF-magnetron sputtered  $\text{Al}_2\text{O}_3$  gate (2.97 eV)

than ALD Al<sub>2</sub>O<sub>3</sub> gate (2.20 eV) on GaN substrate<sup>3</sup> and the acquisition of a better  $J$ - $E$  characteristics as shown in Figure 1. It has been reported that the presence of dangling bonds on the surface of GaN substrate will act as electrically active defects.<sup>19,20</sup> These active defects will form defect states within the band gap of the GaN substrate that leads to high leakage current. Initially, these defect states will capture the injected electrons from valence band of the substrate and act as scattering centers. These scattering centers will stimulate injection of electrons to overcome the conduction band of the substrate. Therefore, the presence of electrically active defects on the surface of GaN substrate needs to be passivated by Al<sub>2</sub>O<sub>3</sub> gate to become passive defects and improved the  $J$ - $E$  characteristic. Besides, the good interface quality of RF-magnetron sputtered Al<sub>2</sub>O<sub>3</sub> gate on GaN substrate ( $D_{it} = 1.1 \times 10^{13} \text{ cm}^{-2} \text{ eV}^{-1}$  at  $E_c - E_t = 0.50 \text{ eV}$ ), which is comparable with the atomic layer deposited (ALD) Al<sub>2</sub>O<sub>3</sub> gate on GaN substrate ( $D_{it} = 1.0 \times 10^{13} \text{ cm}^{-2} \text{ eV}^{-1}$  at  $E_c - E_t = 0.50 \text{ eV}$ )<sup>3</sup> further supports that the Al<sub>2</sub>O<sub>3</sub> gate has passivated the surface of GaN substrate. Moreover, a good oxide quality is of importance to determine good passivation behavior of the Al<sub>2</sub>O<sub>3</sub>. This has been demonstrated through the acquisition of positive  $Q_{\text{eff}}$  in the Al<sub>2</sub>O<sub>3</sub> that has assisted in enhancing the  $J$ - $E$  characteristic. The presence of positive  $Q_{\text{eff}}$  would assist in capturing the injected electrons to form neutral traps instead of breaking the network of Al<sub>2</sub>O<sub>3</sub>. Hence, a higher  $E$  is needed to break the network of Al<sub>2</sub>O<sub>3</sub> as well as to detrapp charges from the neutral traps via PF emission.

## CONCLUSION

In conclusion, an ultrathin polycrystalline Al<sub>2</sub>O<sub>3</sub> gate deposited on GaN substrate was successfully formed at 800 °C in O<sub>2</sub> ambient. MOS characteristics of Al/Al<sub>2</sub>O<sub>3</sub>/GaN were reported in this work. Various possible current conduction mechanisms contributing to the leakage current of this sample were identified. These current conduction mechanisms were dependent on measurement temperature.

## AUTHOR INFORMATION

### Corresponding Author

\*E-mail: cheong@eng.usm.my. Tel: +604-599 5259. Fax: +604-594 1011.

### Notes

The authors declare no competing financial interest.

## ACKNOWLEDGMENTS

H.J.Q. acknowledges financial support given by Universiti Sains Malaysia, The USM RU-PRGS (8044041), and The Universiti Sains Malaysia Vice Chancellor's Award.

## REFERENCES

- (1) Chang, S. J.; Wang, C. K.; Su, Y. K.; Chang, C. S.; Lin, T. K.; Ko, T. K.; Liu, H. L. *J. Electrochem. Soc.* **2005**, *152*, G423–G426.
- (2) Quah, H. J.; Cheong, K. Y. *IEEE Trans. Electron Devices* **2012**, *59*, 3009–3016.
- (3) Hori, Y.; Mizue, C.; Hashizume, T. *Jpn. J. Appl. Phys.* **2010**, *49*, 080201–1–080201–3.
- (4) Ostermaier, C.; Lee, H. C.; Hyun, S. Y.; Ahn, S. I.; Kim, K. W.; Cho, H. I.; Ha, J. B.; Lee, J. H. *Phys. Stat. Sol. (c)* **2008**, *5*, 1992–1994.
- (5) Wu, Y. Q.; Shen, T.; Ye, P. D.; Wilk, G. D. *Appl. Phys. Lett.* **2007**, *90*, 143504–1–143504–3.
- (6) Toyoda, S.; Shinohara, T.; Kumigashira, H.; Oshima, M.; Kato, Y. *Appl. Phys. Lett.* **2012**, *101*, 231607–1–231607–4.

- (7) Cico, K.; Kuzmik, J.; Gregusova, D.; Stoklas, R.; Lalinsky, T.; Georgakilas, A.; Pogany, D.; Frohlich, K. *Microelectron. Reliab.* **2007**, *47*, 790–793.
- (8) Chang, Y. H.; Chiu, H. C.; Chang, W. H.; Kwo, J.; Tsai, C. C.; Hong, J. M.; Hong, M. *J. Cryst. Growth* **2009**, *311*, 2084–2086.
- (9) Chang, Y. C.; Huang, M. L.; Chang, Y. H.; Lee, Y. J.; Chiu, H. C.; Kwo, J.; Hong, M. *Microelectron. Eng.* **2011**, *88*, 1207–1210.
- (10) Basu, S.; Singh, P. K.; Huang, J. J.; Wang, Y. H. *J. Electrochem. Soc.* **2007**, *154*, H1041–H1046.
- (11) Lecce, V. D.; Krishnamoorthy, S.; Esposto, M.; Hung, T. H.; Chini, A.; Rajan, S. *Electron. Lett.* **2012**, *48*, 1–2.
- (12) Hung, T. H.; Krishnamoorthy, S.; Esposto, M.; Nath, D. N.; Park, P. S.; Rajan, S. *Appl. Phys. Lett.* **2013**, *102*, 072105–1–072105–4.
- (13) Nepal, N.; Garces, N. Y.; Meyer, D. J.; Hite, J. K.; Mastro, M. A.; C. R. E., Jr. *Appl. Phys. Exp.* **2011**, *4*, 055802–1–055802–3.
- (14) Schroder, D. K. *Semiconductor Material and Device Characterization*; Wiley: New York, 1998; p 337.
- (15) Quah, H. J.; Cheong, K. Y. *Sci. Adv. Mater.* **2013**, DOI: 10.1166/sam.2013.1647.
- (16) Cheong, K. Y.; Moon, J. H.; Kim, H. J.; Bahng, W.; Kim, N. K. *J. Appl. Phys.* **2008**, *103*, 084113–1–084113–8.
- (17) Quah, H. J.; Cheong, K. Y.; Hassan, Z.; Lockman, Z. *Electrochem. Solid-State Lett.* **2010**, *13*, H116–H118.
- (18) Coan, M. R.; Woo, J. H.; Johnson, D.; Gatabi, I. R.; Harris, H. R. *J. Appl. Phys.* **2012**, *112*, 024508–1–024508–6.
- (19) Moustakas, T. D. In *Gallium Nitride (GaN) II: Semiconductors and Semimetals*; Pankove, J. I., Moustakas, T. D., Eds.; Academic Press: San Diego, 1999; Vol. 57, p 73.
- (20) Lenahan, P. M. In *Defects in Microelectronic Materials and Devices*; Fleetwood, D. M., Pantelides, S. T., Schrimpf, R. D., Eds.; CRC Press: Boca Raton, FL, 2009; p 164.